Soft Matter

PAPER

View Article Online
View Journal | View Issue

Cite this: *Soft Matter*, 2014, **10**, 519

Structural and dynamical properties of reconstituted myelin sheaths in the presence of myelin proteins MBP and P2 studied by neutron scattering

Wiebke Knoll,[ab] Judith Peters,[abc] Petri Kursula,[de] Yuri Gerelli,[b] Jacques Ollivier,[b] Bruno Demé,[b] Mark Telling,[fg] Ewout Kemner[h] and Francesca Natali*[bi]

Received 18th May 2013
Accepted 4th November 2013

DOI: 10.1039/c3sm51393a

www.rsc.org/softmatter

The myelin sheath is a tightly packed, multilayered membrane structure wrapped around selected nerve axons in the central and the peripheral nervous system. Because of its electrical insulation of the axons, which allows fast, saltatory nerve impulse conduction, myelin is crucial for the proper functioning of the vertebrate nervous system. A subset of myelin-specific proteins is well-defined, but their influence on membrane dynamics, i.e. myelin stability, has not yet been explored in detail. We investigated the structure and the dynamics of reconstituted myelin membranes on a pico- to nanosecond timescale, influenced by myelin basic protein (MBP) and myelin protein 2 (P2), using neutron diffraction and quasi-elastic neutron scattering. A model for the scattering function describing molecular lipid motions is suggested. Although dynamical properties are not affected significantly by MBP and P2 proteins, they act in a highly synergistic manner influencing the membrane structure.

1. Introduction

Myelin is the insulating, multi-lamellar membrane structure that surrounds selected nerve axons in both the central nervous system (CNS) and the peripheral nervous system (PNS). Its main function is the electrical insulation of the axons and it accelerates the nerve impulse transmission.

Compared to an average cellular membrane, myelin is very lipid-rich, containing 75–80% anionic and neutral lipids and only 20–25% proteins.[1] The major lipids in CNS and PNS myelin are cholesterol, phospholipids, and galactolipids, which are important for the membrane structure and assembly.[2,3] CNS and PNS myelin contain different unique proteins, which interact closely with the membrane.[4–6] The major CNS compact myelin proteins are MBP, which accounts for ~30%,[7] and proteolipid protein (PLP), which constitutes ~50% of the total protein fraction.[8] PNS myelin contains MBP (present at only 5–18%[7]), the P0 glycoprotein, the peripheral myelin P2, and the peripheral myelin protein-22 (PMP-22). In this study, model membranes mimicking the PNS compact myelin, which contain both MBP and P2, were investigated, and particularly, the influence of the proteins on membrane dynamics was assessed.

MBP, which is located between the cytoplasmic leaflets of compact myelin, is one of the main agents responsible for formation and compaction of CNS myelin and maintains myelin stability.[9–11] The most abundant isoform of human MBP is the 18.5 kDa protein. A precise three-dimensional structure of MBP is unknown; due to intramolecular electrostatic repulsion (net charge of +20 at neutral pH) and the lack of a hydrophobic core, it exists in an extended, intrinsically disordered conformation in solution.[12–15] In contrast, in the presence of lipids, MBP adopts a more ordered structure with α-helices and β-sheets.[14,16,17] Based on electron microscopy single particle reconstructions and molecular dynamics simulations, a "C"-shape with a β-backbone was suggested for lipid-bound bovine MBP,[18,19] as illustrated in Fig. 1(a) (Protein Data Bank entry 1QCL).

MBP most likely lies flat in the major dense line of myelin, penetrating deeply into opposing bilayers. The region consisting of the residues 83–92 of recombinant murine MBP was found to form an α-helix when bound to myelin-like vesicles, penetrating into the lipids.[21,22] Also other membrane-binding segments have been characterized. MBP binds to mixtures of neutral and anionic lipids, preferentially to the latter.[14,23,24] The 14.8 kDa P2 protein is only present in the PNS, constituting 1–15% of the total protein fraction, depending on the species.[2,6,25] Like MBP, it is located on the cytoplasmic side of compact myelin.[26] The

[a]*University Joseph Fourier UFR PhITEM, Grenoble, France*
[b]*Institut Laue–Langevin, Grenoble, France. E-mail: natali@ill.fr*
[c]*Institut de Biologie Structurale, Grenoble, France*
[d]*Department of Biochemistry & Biocenter Oulu, University of Oulu, Oulu, Finland*
[e]*Department of Chemistry, University of Hamburg & CSSB-HZI/DESY, Hamburg, Germany*
[f]*ISIS Facility, Rutherford Appleton Laboratory, Didcot, UK*
[g]*Department of Materials, University of Oxford, Oxford, UK*
[h]*Helmholtz-Zentrum Berlin für Materialien und Energie GmbH, Berlin, Germany*
[i]*CNR–IOM–OGG, c/o Institut Laue–Langevin, Grenoble, France*

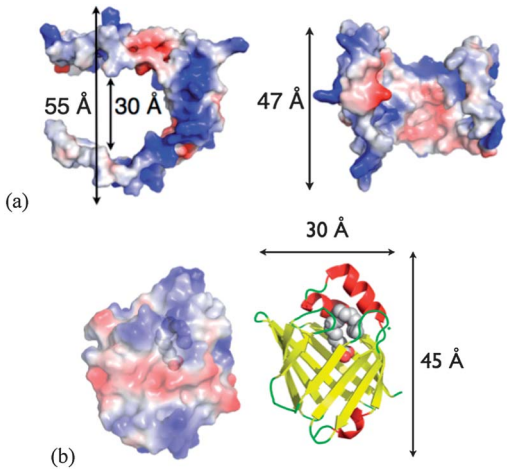

Fig. 1 (a) "C"-shape of bovine MBP determined by electron microscopy and molecular modeling.[18,19] (b) Left: electrostatic potential of the human P2 surface (blue: positive charge; red: negative charge; grey: neutral). Right: crystal structure of human P2.[20] The bound palmitate molecule in the crystal structure is shown as spheres.

electrostatic surface distribution of P2 (net charge +10 at neutral pH), with two opposed highly positively charged regions separated by a neutral, central rim (Fig. 1(b), left), allows the protein to interact with two apposing myelin leaflets.[20] P2 has been suggested to have a similar structural function in PNS myelin as MBP in CNS myelin; this is supported by the notion that MBP-deficient mice have essentially normal-looking myelin in the PNS, even though CNS myelination is severely impaired.[27,28] Furthermore, atomic force microscopy (AFM) studies[29] indicated that MBP and P2 present together in a membrane surface have a cooperative action to induce stacking of bilayers into multilayers. The structure of human P2 was determined by X-ray crystallography,[20] revealing a compact β-barrel, which consists of 10 antiparallel β-sheets surrounding a ligand-binding cavity inside the barrel (Fig. 1(b), right). On top of the barrel, two α-helices are located like a lid, which may open when the internal binding cavity interacts with lipids, and it probably penetrates into the membrane.[30] Like MBP, the structure of P2 changes when bound to lipids, resulting in a decrease in the α-helical and an increase of the β-sheet content.[31] Previous neutron scattering studies have shown that P2 bound to myelin-mimicking vesicles either made of 1,2-dimyristoyl-*sn*-glycero-3-phosphatidic acid (DMPA) or of a binary mixture of 1,2-dioleoyl-*sn*-glycero-3-phospho-L-serine (DOPS) and 1,2-dioleoyl-*sn*-glycero-3-phosphocholine (DOPC), respectively, reduces the lipid dynamics.[32]

In the present study, the influence of MBP and P2 on the structure and the dynamics of myelin model membranes was investigated, using neutron diffraction and quasi-elastic neutron scattering. The neutron scattering technique is a powerful tool for the investigation of biological macromolecules, since they contain approximately 50% hydrogen atoms with a very large incoherent cross-section compared to other elements. The energies and wavelengths of cold and thermal neutrons ranging from 0.1 to 100 meV and from 1 to 30 Å, respectively, allow the investigation of molecular motions occurring on a pico- to nanosecond timescale and on an atomic length-scale. Model membranes were reconstituted from a binary mixture of two synthetic lipids (anionic DOPS and neutral DOPC) and the myelin proteins MBP and P2 were used to mimic the cytoplasmic leaflet of the highly complex natural myelin membrane. With this anionic-neutral lipid composition it was possible to imitate negatively charged compact myelin, which mainly contains phospholipids (40% of total dry weight), cholesterol (30%) and galactolipids (30%). Since the purpose of the experiments was to study the properties of the myelin-like membranes in their gel and in their liquid phases, and as the melting temperature of human P2 is $T_M = 335$ K,[20] DOPS and DOPC are very suitable due to their low phase transition temperatures ($T_C = 262$ K for DOPS and $T_C = 253$ K for DOPC). DOPS and DOPC both possess the same hydrophobic tails containing 18 carbon atoms in each fatty acyl chain, but different hydrophilic headgroups.

2. Materials and methods

2.1. Sample preparation and characterization

Recombinant His_6-tagged murine 18.5 kDa MBP was expressed in *Escherichia coli* (*E. coli*) BL21(DE3) cells using the pET-22b vector and IPTG induction, and purified using immobilized metal ion chromatography under denaturing conditions as previously described.[33,29] His_6-tagged human P2 was expressed by the autoinduction method[34] in *E. coli* Rosetta(DE3) cells, using the pTH27 vector,[35] and purified as reported in ref. 20. Both proteins were dialyzed against a buffer containing 20 mM HEPES (pH 7.5) and 150 mM NaCl. The purity of the preparations was verified by sodium dodecyl sulfate polyacrylamide gel electrophoresis (SDS-PAGE), and concentrations were determined using UV absorbance at 280 nm and calculating theoretical extinction coefficients.

For the preparation of the reconstituted membranes, DOPS and DOPC lipids were purchased from Avanti® Polar Lipids (Alabaster, AL, USA) and used without further purification (purity of at least 99%). For multilamellar vesicle formation, the lipid powders were dissolved and mixed in chloroform with a 1 : 1 mass ratio. Chloroform was removed to yield a thin lipid film, using a dry nitrogen stream. The lipids were further dried under vacuum overnight and subsequently hydrated in D_2O (concentration of 50 mg ml^{-1}), resulting in large multilamellar vesicles (LMVs). D_2O was used for hydration due to the very small incoherent cross-section of deuterium, in order to change the contrast between solvent and lipids. After 5 cycles of freezing and thawing of the LMV suspension, large unilamellar vesicles (LUVs) were obtained by extrusion through a 100 nm pore-sized membrane, using the Avanti® Mini-Extruder. Appropriate amounts of protein solution, at a concentration respecting the protein ratio of MBP and P2 in the PNS, were added to the LUV solution. The concentration of MBP was 0.14 mg ml^{-1}, resulting in 0.28% (w/w) with respect to the reconstituted membrane and the concentration of P2 was 0.31 mg ml^{-1}, corresponding to 0.62% (w/w). First of all, this very small protein amount was adequate to observe possible variations of the membrane dynamics due to the presence of proteins, without contributions arising from the protein dynamics.

Moreover, the chosen protein concentration allowed us to eliminate experimental artifacts arising from lipid-aggregation at higher protein quantities. Recent studies of Patzig *et al.*[6] revealed quantities of MBP and P2 of 2% and 0.5% of total PNS myelin by mass spectrometric quantification. The protein-to-lipid molar ratio was, thus, approximately 1 : 8000 for MBP and 1 : 3000 for P2. The following samples were prepared: protein-free lipids (named pf-lipids in the following), lipids with MBP (named MBP–lipids), lipids with P2 (named P2–lipids) and lipids with MBP and P2 (named MBP–P2–lipids). The LUV suspensions were spread on SiO_2 (1 1 1) wafers (Silchem, Freiberg, Germany) to promote the formation of oriented multilayers. The samples were dried in a vacuum oven for 24 h and then re-hydrated in a D_2O atmosphere with a relative humidity of 95%, using a saturated $CaSO_4$–D_2O solution, for 36 h. At this high hydration level, which was the same for all samples, the number of D_2O molecules per lipid molecule can be estimated to be 25 to 27.[66] The incoherent scattering cross-sections of water and lipids were evaluated to 1.7% and 98.3%. For simplification purposes, we can exclude any contribution of the D_2O to the scattered intensities. Three such wafers were stacked in an aluminium sample holder with an empty wafer on the top, and each wafer contained approximately 33 mg of lipids. Since the success of the neutron scattering experiments and the reliability of the results depend on the quality of the samples, detailed sample characterization was performed with a range of biophysical techniques, as described in detail in another following paper. Dynamic light scattering (DLS) experiments were performed in order to determine the particle size-distribution of the LUV solution with and without proteins. Sucrose gradient centrifugation followed by SDS-PAGE was used to verify the lipid–protein binding. Therefore, the sample of each protein–LUV solution was applied on the top of the gradient and was ultra-centrifuged. This allowed identifying possible lipid or protein aggregates, which are not bound to the lipids, since those would travel to the bottom of the gradient having a high density. Each sucrose layer was further analyzed by SDS-PAGE. As shown in Fig. 2, proteins were present only in the lipid–protein sample (and not in the sucrose layers), which indicated that they are bound to the lipids. Differential scanning calorimetry (DSC) experiments confirmed the presence of two distinct gel-to-liquid phase transitions of both lipids at the expected temperatures T_c. Finally, neutron diffraction experiments on D16 (Institut Laue-Langevin, ILL, Grenoble, France) on the final membrane samples for the investigation of the characteristic repeat distance and the mosaic spread of the membrane indicated highly parallel oriented multilayers: each wafer was then estimated to contain ~6600 bilayers with a mosaic spread of less than 0.5 degrees.

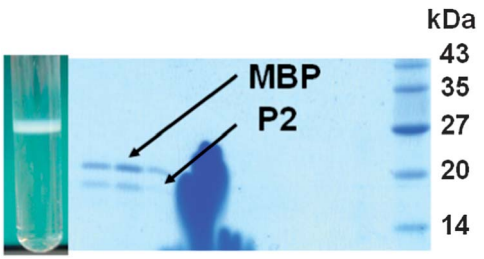

Fig. 2 Verification of lipid–protein binding: SDS-PAGE for samples of the sucrose gradient with lipid-band and myelin proteins MBP and P2 after centrifugation (inset). Protein bands of MBP (18.5 kDa) and P2 (14.8 kDa) are clearly visible in gel-columns with the lipid–protein band of the gradient, indicating correct lipid–protein binding. (The "flower" at the bottom of the gel is a typical feature assigned to lipids).

2.2. Neutron diffraction and quasi-elastic neutron scattering

Neutron diffraction measurements were performed on the diffractometer D16[36] and the backscattering spectrometer IN16,[37] having supplementary diffraction detectors, at the ILL (Grenoble, France), which allowed the investigation of the membrane structure in a very large Q-range. Since the Q-region explored on D16 was 0.04 $Å^{-1} \leq Q \leq 0.42$ $Å^{-1}$, repeat distances characteristic for the reconstituted DOPS–DOPC bilayers were investigated. Moreover, with an accessible Q-range on IN16 of 0.36 $Å^{-1} \leq Q \leq 1.84$ $Å^{-1}$, Bragg peaks characteristic for ice, which was present in the fully hydrated membranes, were visible. In order to cover the gel-to-liquid phase transitions of the lipids, elastic temperature scans, ranging from 240 K to 300 K and back, were performed on D16 and from 20 K to 300 K on IN16.

To investigate molecular motions of the lipids occurring over a very broad temporal range and on different length-scales, influenced by MBP and P2, quasi-elastic neutron scattering (QENS) experiments were carried out on the three time-of-flight spectrometers IN5 (ILL, Grenoble, France), Osiris (ISIS at the Rutherford Appleton Laboratory, Oxfordshire, United Kingdom) and Neat (Helmholtz-Zentrum Berlin, Berlin, Germany) with different energy resolutions and Q-ranges. For IN5 an energy resolution (FWHM) of 12 μeV (corresponding to a timescale of ~30 ps), for Osiris of 100 μeV (~10 ps) and for Neat of 216 μeV (~1 ps), was used. With Q-ranges of 0.1 $Å^{-1} \leq Q \leq 1.14$ $Å^{-1}$ for IN5, 0.60 $Å^{-1} \leq Q \leq 3.52$ $Å^{-1}$ for Osiris and 0.37 $Å^{-1} \leq Q \leq 2.26$ $Å^{-1}$ for Neat, the identification of membrane dynamics of different length-scales was possible: 5.5 Å $\leq d \leq$ 62.8 Å (IN5), 1.8 Å $\leq d \leq$ 10.5 Å (Osiris) and 2.8 Å $\leq d \leq$ 17.0 Å (Neat), with $d = 2\pi/Q$. The measurements were performed at 300 K, corresponding to the liquid phase of both lipids. In order to study molecular motions predominantly parallel (in-plane) and perpendicular (out-of-plane) to the membrane plane, samples were oriented at 135° and at 45° with respect to the incoming neutron beam, as illustrated in Fig. 3.

For correction purposes, a cell with four SiO_2 wafers, a vanadium sample and an empty cell were measured at 300 K. With a transmission of the samples of ~95%, multiple scattering effects could be neglected. Data corrections were performed using ILL software LAMP for IN5 data,[38] ISIS software MODES for Osiris data[39] and HZB software FITMO[40] for Neat data. After subtraction of a spectrum of the empty cell with wafers from the data, the spectra were normalized to the scattering signal of vanadium to compensate for spurious background anomalies and detector efficiency. The Q-values for the membrane Bragg peaks, as well as the Q-values containing the

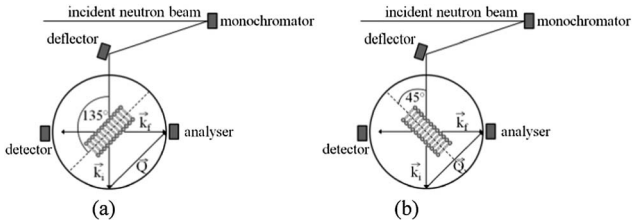

Fig. 3 Scheme of the two orientations of the membrane samples in the geometry of the backscattering spectrometer IN16: (a) in-plane configuration: the sample is oriented at 135° with respect to the incoming beam; the scattering vector Q is parallel to the membrane plane. (b) Out-of-plane configuration: the sample is oriented at 45° and Q is perpendicular to the membrane plane.

shadow of the sample holder present at the out-of-plane configuration, were excluded.

2.3. Quasi-elastic data analysis

The theoretical scattering function describing a quasi-elastic spectrum can be written in general as[41]

$$S_{\text{theo}}(Q,\omega) = \mathrm{e}^{-\langle u^2\rangle Q^2}\left[A_0\left(\vec{Q}\right)\delta(\omega) + \sum_n A_n(Q)L_n(Q,\omega)\right], \quad (1)$$

where the first term is analogous to the Debye–Waller factor used in crystallography to describe atomic vibrations. The delta function takes into account atoms performing motions that cannot be resolved within the instrumental energy resolution and appear immobile and A_0 is the elastic incoherent structure factor, which is the fraction of the elastic contribution contained in the total scattering intensity. The last term is the quasi-elastic component of the scattering function, which consists of a sum of Lorentzians, describing the identified molecular motion. The Q-dependent functions $A_n(Q)$ are the quasi-elastic structure factors, which give the relative intensities of quasi-elastic contributions.

In order to describe molecular motions in the reconstituted membrane samples, the measured quasi-elastic spectrum was modelled by the theoretical model function $S_{\text{theo}}(Q,\omega)$ and a background B(Q,ω), convoluted with the resolution function $S_{\text{Res}}(Q,\omega)$ of the instrument:

$$S_{\text{meas}}(Q,\omega) \propto [S_{\text{theo}}(Q,\omega) + B(Q,\omega)] \otimes S_{\text{res}}(Q,\omega) \quad (2)$$

The shape of $S_{\text{theo}}(Q,\omega)$ depends on the type of motions, which are very diverse in biological molecules.

A model for $S_{\text{theo}}(Q,\omega)$, which describes five proton populations ("hydrogen atom populations" is used in the following), executing different kinds of motions, has been adopted for our data:

(1) A population that appears immobile within the energy resolution in the quasi-elastic region and that only contributes to the Debye–Waller factor $\exp(-\langle u^2\rangle Q^2)$ with the mean square displacements $\langle u^2\rangle$ by their vibrational motion.

(2) A population undergoing free diffusion in a confined spherical volume of the radius R_{V1} with the diffusion constant D_{V1}, described by the scattering law[42]

$$S_{\text{V1}}(Q,\omega) = A_0(Q)\delta(Q)\delta + \frac{1}{\pi}\sum_{\{l,n\}\neq\{0,0\}}(2l+1)A_n{}^l(Q)\frac{\left(x_n{}^l\right)D_{\text{V1}}/{R_{\text{V1}}}^2}{\left[\left(x_n{}^l\right)^2 D_{\text{V1}}/{R_{\text{V1}}}^2\right]^2+\omega^2} \quad (3)$$

$A_0(Q)$ is the elastic incoherent scattering factor (EISF) and is described by a spherical Bessel-function of first order $j_1(QR_{\text{V1}})$: $A_0(Q) = [3j_1(QR_{\text{V1}})/QR_{\text{V1}}]^2$.

(3) A population undergoing the same motions like 2, with a larger diffusion constant $D_{\text{V2}} > D_{\text{V1}}$ and a radius of confinement R_{V2}.

(4) A population that performs a 2-site jump diffusion among two equivalent sites.[43] This motion is independent from the diffusion in confinement and is faster, causing a much broader quasi-elastic contribution to the spectrum. It is described by

$$S_{\text{Jump}}(Q,\omega) = B_0(Q)\delta(\omega) + [1-B_0(Q)]\frac{1}{\pi}\frac{2\tau_{\text{Jump}}}{4+\omega^2{\tau_{\text{Jump}}}^2} \quad (4)$$

with the EISF $B_0(Q) = 1/2[1 + j_1(Qd)]$, the jump distance d and the mean residence time τ_{Jump} of an atom at one of the equilibrium positions.

(5) An additional Lorentzian had to be added for data obtained on Neat with a large energy resolution (216 μeV), for $Q \leq 0.76$ Å^{-1}. This Lorentzian is constant in Q and describes a motion occurring on a picosecond timescale and on a length-scale of ~10 Å, but its meaning is not clear yet. For a better understanding, experiments on instruments with a similar energy resolution (216 μeV) and a higher Q-resolution for low Q-values would have to be performed. Besides the MBP-sample, the resulting values of the HWHM of this Lorentzian Γ were similar to the HWHM of the 2-site jump diffusion: $2/\Gamma_{\text{Jump}}$. Hence, this Lorentzian could describe a rotational motion that is not included within this model.

The fractions of hydrogen atoms belonging to populations (1) to (5) are indicated by f (1), p_{V1} (2), p_{V2} (3), p_{Jump} (4) and p_{Lor} (5) with $f + p_{\text{V1}} + p_{\text{V2}} + p_{\text{Jump}} + p_{\text{Lor}} = 1$. Hence, the resulting model scattering function is

$$S_{\text{theo}}^{300\text{ K}}(Q,\omega) = \mathrm{e}^{-\langle u^2\rangle Q^2}[f\delta(\omega) + p_{\text{V1}}S_{\text{V1}}(Q,\omega) + p_{\text{V2}}S_{\text{V2}}(Q,\omega) + p_{\text{Jump}}S_{\text{Jump}}(Q,\omega) + P_{\text{Lor}}L_{\text{Lor}}(Q,\omega)] \quad (5)$$

It is important to remark that the Debye–Waller factor is an overall factor common to all of these hydrogen populations.

Since the required quasi-elastic contributions are numerous, the following strategy was used in order to safely reduce the number of fitting parameters: instead of fitting each spectrum individually, a program has been used, which is able to fit simultaneously all spectra at different Q-values obtained on several instruments. This approach was derived for the analysis of QENS dynamics in lipid vesicles by Gerelli *et al.*;[44] the analysis is based on the *Minuit non-linear minimization routine*.[45] Since this routine was written for the use of two instruments, the fitting procedure was performed as follows: IN5 and Osiris data were first fitted. Then, Osiris and Neat data were fitted with fixed parameters of S_{V1}, which were obtained from the first fit. At the last step, IN5 and Osiris data were re-fitted, fixing parameters of

S_{V1}, S_{V2} and S_{Jump}. The additional Lorentzian was adjusted in the last step by fitting the first four Q-groups of Neat-data with fixed parameters for S_{V1}, S_{V2} and S_{Jump}. The pre-factors f, p_{V1}, p_{V2} and p_{Jump} were not the same for all instruments, since the model is an average description of the main motions, but does not contain information about all components present in the system, for example water. Hence, scattering intensities arising from some of these components are considered negligible when analyzing the data of the single instruments, but they lead to differences when fitting all the instruments together.

3. Results and discussion

3.1. Structural properties of the membranes

The structure of the multilayered membranes was studied using neutron diffraction as a function of temperature (Fig. 4).

For the pf-lipids, repeat distances of ~59 Å were obtained for both the gel and the liquid phase (Fig. 4 and 5). In contrast, this repeat distance shifted to smaller values at ~262 K, when the lipids have transformed to the liquid phase, but the water has not melted yet, and shifted back to the initial distance, at the melting point of the D_2O, at ~277 K. This behavior could be explained as follows. Assuming that the confined hydration water in the membrane is amorphous, it could be squeezed out of the membrane and become ice, when both lipids have transformed from the gel to the liquid phase (at ~262 K), resulting in a smaller repeat distance. In the diffraction pattern (Fig. 4(a)) this is visible as a jump-like decrease. When the ice becomes liquid, it probably moves into the interbilayer space again and the repeat distance increases slowly to the initial value (~59 Å). The fact that the repeat distance in the liquid phase is the same as in the gel phase, and not smaller (which would be expected since liquid D_2O has a smaller volume than ice), could indicate that the water is in its amorphous state. Related findings have been made by Weik *et al.*[67] Fig. 4(b) illustrates a diffraction pattern obtained on IN16. Three Bragg peaks were obtained at 1.6, 1.7 and 1.8 $Å^{-1}$, which are characteristic for hexagonal ice, and which disappear at the water melting point, indicating that there is bulk D_2O outside the membrane.[46–49]

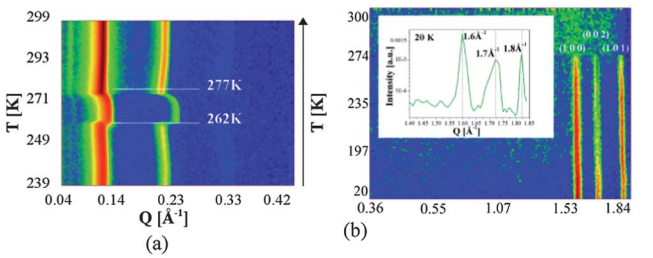

Fig. 4 (a) Diffraction patterns obtained on D16 for the pf-lipids during heating. The color represents the radially summed scattering intensity as a function of Q and of the temperature. A shift of the repeat distance of the bilayers is visible with increasing temperature. (b) Diffraction patterns obtained on IN16 for the pf-lipids during heating. The inset shows the three Bragg peaks obtained at 1.6, 1.7 and 1.8 $Å^{-1}$, at 20 K, assigned to crystalline water.

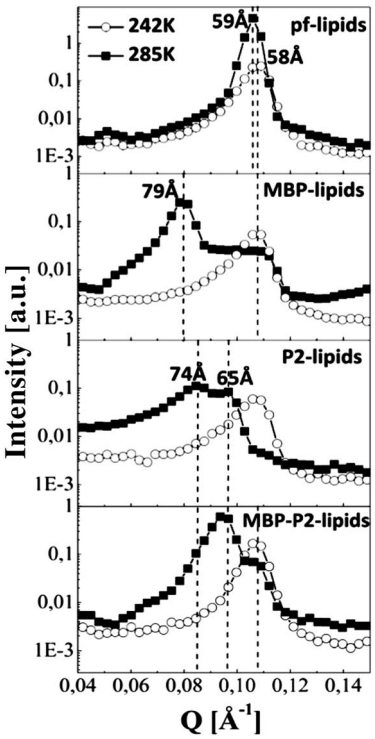

Fig. 5 Diffraction patterns for pf-lipids (a), MBP–lipids (b), P2–lipids (c) and MBP–P2–lipids (d) at 242 K (lipid gel phase, represented by the open circles) and at 285 K (lipid liquid phase, represented by the filled squares) achieved on D16.

Fig. 5 shows the Q-dependent diffraction patterns for all samples at 242 K (below the lipid phase transitions) and at 285 K (above the lipid phase transitions). In the gel phase, all samples show the same repeat distance. Nevertheless, the Bragg peak is less intense and broader for the MBP– and the P2–lipids than for the other samples, suggesting a more disordered structure. Furthermore, the intercept is higher, suggesting a less ordered membrane fraction with a large d-spacing (corresponding to low Q-values), which cannot be resolved here. Since MBP is known to be squeezed out of a bilayer in the gel phase, and preferentially binds to lipids in the liquid phase,[50,51] this domain could be associated with areas of squeezed out proteins. In contrast, for the MBP–P2–lipids this effect seems to be compensated by the presence of the two proteins (intercept dimension as for pf-lipids), which could be caused by the stacking effect of MBP and P2.[29] For the liquid phase, additional Bragg peaks arise, when myelin proteins are present: the MBP– and the MBP–P2–lipids show both the d-spacing characteristics for the pf-lipids and other repeat distances, indicating the formation of lipid domains with and without proteins (Fig. 5(b) and (d)). However, the P2–lipids exhibit two repeat distances in the liquid phase, which are larger than for the pf-lipids (Fig. 5(c)). To better understand how the proteins are organized within the membrane, these Bragg peaks were fitted with Gaussian functions and gave rise to the following structural models in the lipid liquid phase.

For the pf-lipids the fitting gave a repeat-distance of 59 Å, as shown in Fig. 6(a). With a bilayer thickness of ~37 Å for a DOPS–DOPC-bilayer,[52,53] the interbilayer spacing is ~22 Å. This

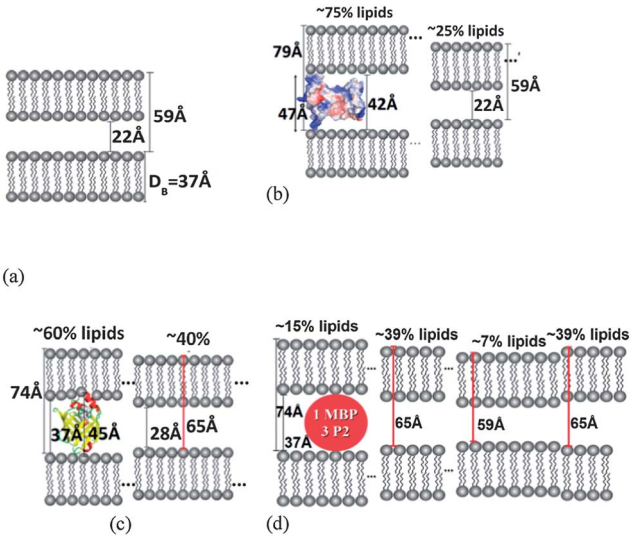

Fig. 6 Schematic views of DOPS–DOPC membranes with, and without, proteins. (a) Protein-free membrane unit: the same repeat distance of ~59 Å was obtained in both the gel and the liquid phases of the lipids. D_B: average bilayer thickness. (b) Membrane unit containing an MBP protein. Membrane fractions affected by MBP account for ~75%. (c) Membrane unit containing a P2 protein, completely affected by P2. (d) Membrane unit containing both MBP and P2 proteins, where a membrane fraction of only ~7% remains unaffected.

distance is likely to be affected by electrostatic repulsion between the apposed membranes.

For the MBP–lipids, the protein-free membrane fraction accounts for ~25% and the fraction containing MBP for ~75% (Fig. 6(b)). With a repeat distance of 79 Å, the C-shaped MBP fits between the bilayers by penetrating ~2 Å at each side into the bilayer, maybe executed by the α-helical residues 83–92 of the protein.[21,22] It should be noted that the C-shape was determined on lipid monolayers, and the conformation between two bilayers may be different.

For the P2–lipids, a fraction with a repeat distance of ~74 Å was found to account for ~60% and the fraction with a *d*-spacing of ~65 Å for ~40%, as illustrated in Fig. 6(c). Since the height of the β-barrel is ~30 Å, and the diameter of the entire P2 crystal structure 45 Å, we assume that the protein is located in membrane fractions with the larger *d*-spacing, and the α-helical lid probably penetrates deeply into the bilayer. Membrane fractions with a repeat-distance of 65 Å probably show an intermediate distance between protein-affected and protein-unaffected membrane fractions.

For the MBP–P2–lipids (Fig. 6(d)), three repeat distances of ~59 Å (protein-unaffected), ~74 Å and ~65 Å (as for the P2–lipids) were identified. Because of a threefold higher amount of P2 proteins than MBP proteins in the MBP–P2–lipids, it is possible that proteins synergistically build assemblies within the membrane (Fig. 6(d)). This hypothesis is one possible assumption and probably the simplest case. Since we did not find any repeat-distance characteristic for the MBP-sample (79 Å), it seems that P2 dictates the dimension in the protein-containing membrane domain of 74 Å. MBP would have to penetrate deeply into the bilayers with its height of 47 Å in the C-shaped conformation; it could also take a more flat conformation in the presence of P2. The unaffected membrane-fraction accounts only for 7%.

Surprisingly, we found that the protein-free membrane fraction became very low in the presence of such a small protein amount, although the fraction of surface with protein-bound lipids can be calculated to 0.31% for the MBP–lipids, 0.23% for the P2–lipids and 0.53% for the MBP–P2–lipids. Fig. 7 shows a scheme of the surface contribution of protein-bound lipids for the MBP–P2–lipids. A possible explanation are strong electrostatic interactions between the P2 protein and the negatively charged lipids, because P2 has a high positive electrostatic potential at the two opposing sides of the protein, separated by a neutral central rim. These interactions seem to be long-range and thus influence large membrane fractions.

3.2. Dynamical properties of the membranes

Fig. 8 shows quasi-elastic spectra of all samples measured on IN5 at 300 K for the in-plane configuration (left) and the out-of-plane configuration (right), normalized and integrated over the whole accessible *Q*-range.

For both, small differences in the quasi-elastic broadening are visible. Fig. 9 illustrates an example for the fitting of

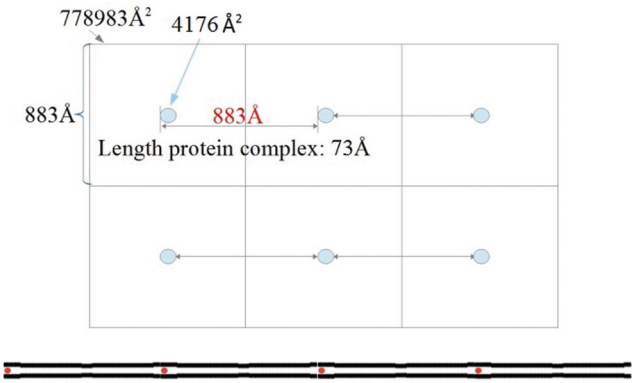

Fig. 7 Scheme of the surface contribution of lipid-bound proteins in a monolayer of the MBP–P2–lipids. Top: top view; bottom: side view. The fraction of the surface with protein-bound lipids was calculated to be 0.53%.

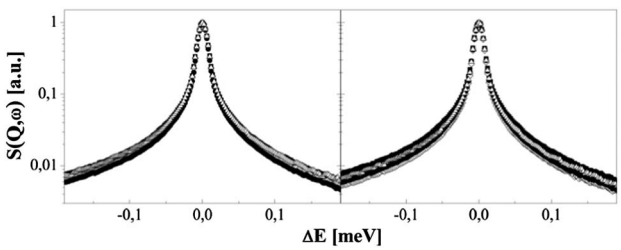

Fig. 8 Quasi-elastic spectra of pf-lipids (filled circles), MBP–lipids (open triangles), P2–lipids (filled squares) and MBP–P2–lipids (open rhombs) measured on IN5 at 300 K. Data are shown for in-plane configuration (135°, left) and out-of-plane configuration (45°, right). The normalized intensities were integrated over the whole accessible *Q*-range.

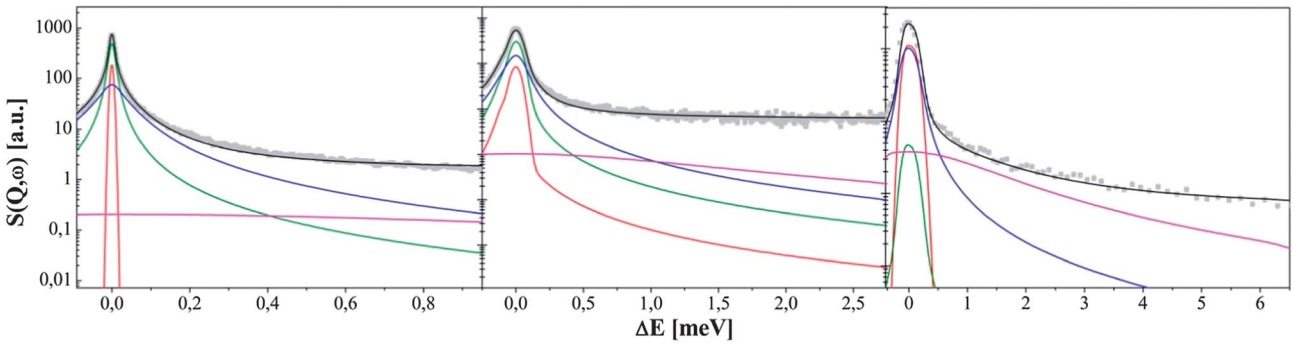

Fig. 9 Normalized quasi-elastic data for pf-lipids in the out-of-plane configuration at 300 K, fitted using eqn (5). Data (grey squares) are shown for $Q \approx 0.9$ Å^{-1} and plotted together with the total fit function (black), $S_{V1}(Q,\omega)$ (green), $S_{V2}(Q,\omega)$ (blue), the 2-site jump diffusion (magenta) and the elastic line (red), which is the resolution function. Left: IN5-data; middle: Osiris-data; right: Neat-data.

quasi-elastic spectra obtained from the pf-lipids at 300 K in the out-of-plane configuration for all instruments at similar Q-values, using eqn (5).

Results for the fitting parameters R_V, D_V, d, τ_{Jump} and Γ are given in Table 1, where the index 1 stands for $S_{V1}(Q,\omega)$ and index 2 for $S_{V2}(Q,\omega)$. The hydrogen fraction p_{Jump} performing 2-sites jump diffusion (magenta curve) is visible only on Neat, accounting for ~50%, and participates as a flat background on IN5 and Osiris spectra, accounting for only 5–10%. In contrast, the fraction p_{V1}, which is related to diffusion in a confined spherical volume of radius R_{V1}, is clearly observable on IN5 and Osiris, representing fractions of 40–50%, but cannot be resolved by the energy resolution of Neat.

The type of dynamics described by the model has already been found in lipid-membranes using quasi-elastic neutron scattering,[44,54–58] NMR studies[59] and molecular dynamics simulations.[60] Brown *et al.*[59] have carried out NMR studies on 1,2-dipalmitoyl-*sn*-glycero-3-phosphocholine (DPPC) and DOPC multilayers as well as on DPPC vesicles, to investigate spin lattice relaxation rates $1/T_1$. The relaxation time T_1, which is the time for the return of the spin from the excited to the equilibrium state, characterizes internal lipid chain dynamics and molecular reorientations of the chain methylenes, occurring on a pico- to nanosecond timescale. These reorientations arise from molecular rotational diffusion or from internal dynamics as torsional isomerization between *gauche* and *trans* conformation. Molecular dynamics simulations indicate that the *trans–gauche* isomerizations occur on a timescale of tens of picoseconds in the lipid chains and slow down closer towards the lipid headgroups (timescale of a few 100 picoseconds).[61] $1/T_1$ relaxation rates as a function of the position along the DPPC lipid chains were found to be constant for the 3rd to the 9th carbon with a frequency of 10^{10}Hz and to increase from the 9th to the 15th carbon. This effect was the same for DPPC multilayers and vesicles. Pitman *et al.*[60] have performed molecular dynamics simulations for T_1 relaxation rates as a function of the carbon positions along the oleic chain of DOPC, which indicated that the relaxation rate is constant from the 1st to the 8th carbon and increases from the 11th to the 17th carbon. At the double bond of the vinyl group, which is between the 9th and 10th carbon of DOPC, the relaxation was slower. This indicated that T_1 spin lattice relaxation rates are strongly affected by unsaturation. Based on these observations, the slow diffusion in confinement (characterized by D_{V1}) performed by population p_{V1} is assigned to the upper part of the lipids (including the lipid head groups and the double bond of the vinyl group) and the fast restricted diffusion executed by p_{V2} to the terminal part of the lipids, from the last methylene group until the double bond. Fig. 10 illustrates schematically the model used to discuss quasi-elastic data obtained for a reconstituted DOPS–DOPC myelin-membrane in the liquid phase.

It summarizes the main motions along the phospholipid molecule, where *f*, the temperature dependent parameter indicating the "immobile" hydrogen atoms, is not included for the

Table 1 Fitting parameters for data obtained at 300 K with the following absolute errors: $\Delta D_{V1} \approx \pm 0.01 \times 10^{-5}$ cm^2 s^{-1}, $\Delta D_{V2} \approx \pm 0.1 \times 10^{-5}$ cm^2 s^{-1}, $\Delta R_{V1} \approx \Delta R_{V2} \approx \pm 1$ Å, $\Delta d \approx \pm 0.5$ Å, $\Delta\tau \approx \pm 0.01$ meV^{-1} and $\Delta\Gamma \approx \pm 0.05$ meV

Sample	R_{V1} [Å]	D_{V1} [cm^2 s^{-1} 10^{-5}]	R_{V2} [Å]	D_{V2} [cm^2 s^{-1} 10^{-5}]	d [Å]	τ_{Jump} [meV^{-1}]	Γ [meV]
Pf-lipids 135°	4	0.16	5	1.8	2.5	0.93	2.15
Pf-lipids 45°	6	0.15	7	1.1	2.5	1.36	1.47
MBP–lipids 45°	5	0.25	5	2.3	2.3	0.80	0.77
MBP–lipids 135°	6	0.17	5	1.8	2.4	1.00	0.52
P2–lipids 45°	5	0.19	7	1.8	2.1	0.92	2.17
P2–lipids 135°	4	0.15	6	1.3	2.5	1.31	1.53
MBP–P2–lipids 45°	4	0.19	6	1.3	2.2	1.32	1.51
MBP–P2–lipids 135°	6	0.16	5	1.7	2.2	1.32	1.52

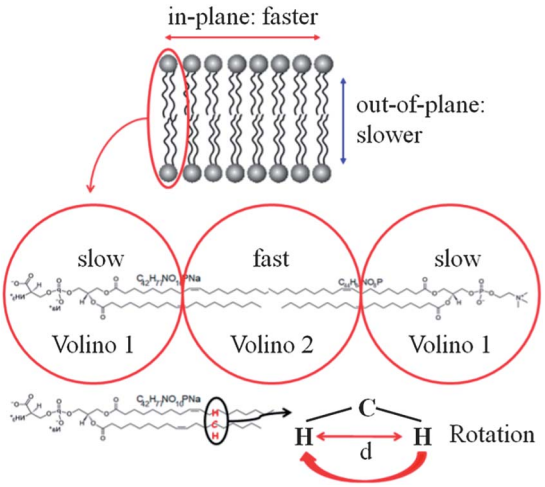

Fig. 10 Schematic illustration of the model applied to quasi-elastic data of a DOPS–DOPC membrane in the liquid phase. $S_{V1}(Q,\omega)$ could be assigned to the initial part of the lipid chains, including the lipid headgroups and the double bond, and $S_{V2}(Q,\omega)$ to the terminal part of the chains, both with a radius of confinement of $R_V \approx 5$ Å. The 2-site jump diffusion could be attributed to the hydrogen-atoms of the methylene groups, with jump distances of $d \approx 1.8$ Å.

sake of clarity. Also p_{Lor} is not indicated, since its origin is still unclear as described above.

It has to be noted that with quasi-elastic neutron scattering, all hydrogen atoms in the samples contribute to the scattering signal resulting in averaged proton dynamics. Thus, we cannot distinguish between membrane domains influenced by MBP and P2 and membrane domains in which the lipids remain unaffected. The observed diffraction data for the same membrane samples revealed that even at these low protein concentrations, the membrane structure is strongly affected by MBP and P2, as described above.

For comparison, the fitting parameter *f*, which represents the contribution of immobile hydrogen atoms obtained on IN5 (left), Osiris (middle) and Neat (right), is illustrated schematically in Fig. 11. There is not much difference for *f* within the error bars between the different samples. The diffusion constants D_{V1} and D_{V2}, describing the fast and slow diffusive processes, differ by one order of magnitude in all samples (illustrated in Fig. 12(a) and (b)), which has also been observed with QENS by Gerelli *et al.*[44] for slow and fast restricted diffusive motions, occurring in LUVs made of 1-palmitoyl-2-oleoyl-*sn*-glycero-3-phosphocholine (POPC) and 1,2-dimyristoyl-*sn*-glycero-3-phospho-L-serine (DMPS) in their liquid phase. The corresponding radii of confinement are shown in Fig. 12(c) and (d).

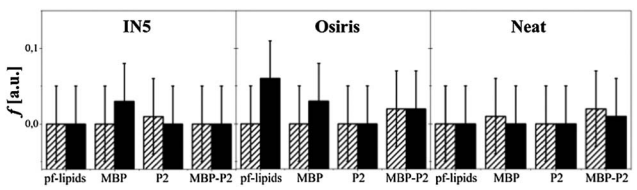

Fig. 11 Fitting parameter *f*, indicating the fraction of immobile hydrogen atoms, obtained for IN5 (left), Osiris (middle) and Neat (right) at 300 K. Half-filled bars: out-of-plane configuration; filled bars: in-plane configuration.

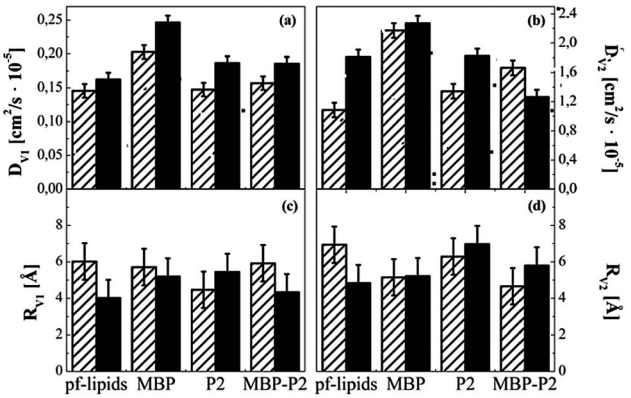

Fig. 12 Diffusion constants D_{V1} (a) and D_{V2} (b) and radii of confinement R_{V1} (c) and R_{V2} (d). Half-filled bars: out-of-plane configuration; filled bars: in-plane configuration.

Regarding the membrane orientations (out-of-plane configuration, half-filled bars and in-plane configuration, filled bars in Fig. 12), the confined diffusion in the initial part of the lipids (D_{V1}) is slightly faster in the in-plane configuration, *i.e.* perpendicular to the lipid chains. This effect is observed in all samples and thus does not seem to be influenced by the myelin proteins in this part of the lipid chains. However, for the diffusion constant D_{V2}, corresponding to the terminal part of the lipids, this tendency is visible for all samples beside the MBP–P2–lipids, which show a faster diffusion in the out-of-plane configuration. The radii of confinement R_{V1} and R_{V2} are approximately 5 Å for all samples (Fig. 12(c) and (d)), according to the radii found by Gerelli and co-workers.[44] Similar values were determined by Doxastakis *et al.*[58] using QENS and molecular simulations on freeze-dried head-deuterated DPPC LUVs in their liquid phase. In contrast, Djurado *et al.*[62] determined several hydrogen atom populations in lipid films that perform diffusion in spheres of different radii.

For the population p_{Jump}, performing 2-site jump diffusion, which was visible mainly on Neat, jump distances *d* between 2.1 Å and 2.5 Å were obtained, with an absolute error of 0.5 Å (Table 1). Within the tolerance, the fraction p_{Jump} could be assigned to CH_2 (methylene) groups in the lipid chains, since the distance between their hydrogens is ~1.8 Å (illustrated in Fig. 10). These dynamics are not to be confused with torsional isomerizations, which have smaller residence times in the order of $\tau_{Jump} = 0.6$ meV^{-1}.[44] Further, they are decoupled from the confined diffusions, because a fitting of a model with a convolution of S_{Jump} and S_{V1} or S_{V2} was not possible with the used instruments. These motions appear decoupled within the time windows we used.

The jump distance does not seem to be influenced by MBP and P2 proteins. However, the residence time τ_{Jump} is larger for the out-of-plane than for the in-plane configuration for all samples, indicating slower jumps in the direction parallel to the lipid chains. For the MBP–lipids τ_{Jump} is smaller for both configurations with respect to the other samples. This suggests

that the methylene groups perform faster jumps, when MBP is bound to the membrane. Also the slow diffusion of fraction p_{V1} is faster when MBP proteins are present in the membrane, compared to the pf-lipids, even more in the in-plane configuration. Regarding the diffusion of fraction p_{V2}, D_{V2} is larger for both configurations. This effect arises together with an increase of the repeat distance of 20 Å of this membrane sample caused by MBP proteins, as measured with neutron diffraction (see above). As illustrated in Fig. 6, we suppose that the protein penetrates 2 Å at each side into the bilayer. The protein-bound membrane fractions accounting for ~75% with respect to protein-free lipid fractions would increase the space for the lipid chains in both directions and hence, the restricted diffusions performed by hydrogen populations in the upper (p_{V1}) and in the lower part of the lipids (p_{V2}), are enhanced for both configurations. The results are related to former studies performed by Natali *et al.*[63–65] on MBP purified from mammalian CNS and bound to a reconstituted oriented membrane made of DMPA: with quasi-elastic and elastic incoherent neutron scattering experiments it was demonstrated that membrane dynamics in the order of 100 ps and 1 ns, characterized by confined diffusive motions of the lipids, were significantly enhanced by MBP in the liquid phase of the lipids, in particular in the out-of-plane configuration. However, the protein concentration was 5 wt% and thus much higher than in our case.

Regarding the P2–lipids, the diffusion coefficients D_{V1} and D_{V2} do not change significantly compared to the pf-lipids, for both configurations. Neutron diffraction on this sample has revealed two widened repeat distances of 65 Å and 74 Å (illustrated in Fig. 5) with respect to the pf-lipids with a *d*-spacing of 59 Å, which could enhance the lipid dynamics. The fraction with the larger interbilayer spacing was suggested to contain P2 proteins, with the α-helical lid (shown in red in Fig. 1) penetrating partially between the lipid headgroups. The fraction with the smaller repeat distance probably depicts an intermediate distance between protein affected and unaffected membrane fractions. However, because of the electrostatic potential of P2, which is highly positive at the two opposing sides of the protein, separated by a neutral central rim, and yields a strong interaction of P2 with negatively charged lipids, this enhancement could be compensated. Additionally, the α-helical lid penetrating partially into the bilayer also might reduce the lipid flexibility. Hence, no differences were obtained in the confined diffusions, with respect to the pf-lipids.

For the MBP–P2–lipids, the diffusion coefficient D_{V2}, which belongs to the terminal part of the lipids, is much smaller with respect to the other samples for the in-plane configuration, indicating a reduction in confined diffusive motions of this lipid part. This effect is in agreement with AFM observations of Suresh *et al.*,[29] which indicate that MBP and P2 synergistically increase membrane stacking, probably caused by an enhancement of the adhesiveness between bilayers due to MBP and P2, which could decrease the motions in this inner part of each bilayer perpendicular to the lipid chains. In contrast, the diffusion constant D_{V1} for the in-plane configuration is of the same order of magnitude as for the pf-lipids, indicating that the restricted diffusion perpendicular to the lipid chains is not affected by the proteins. The hypothesis of MBP–P2–protein assemblies in the membrane, based on neutron diffraction data, is supported by the binding properties of MBP with different cytosolic proteins, which suggests MBP to function as a scaffolding protein.[11] This protein association would cause very strong electrostatic interactions between P2 proteins and the lipid headgroups and the MBP protein would have to penetrate deeply into the bilayer. In contrast to the MBP–lipids and the P2–lipids, a less ordered protein-containing membrane domain with a large repeat distance of ~80 Å was not detected with neutron diffraction. This less ordered domain can be associated with areas of squeezed out proteins, since MBP is known to be squeezed out of a bilayer in the gel phase, and preferentially binds to lipids in the liquid phase.[50,51] The absence of this membrane fraction in the MBP–P2–lipids indicates that all proteins are located in the ordered domains. The unaffected diffusion constant D_{V1} could, similar to the P2-data, also be explained by a compensation effect of the increased mobility due to a widening of the interbilayer spacing and the decreased flexibility caused by strong electrostatic interactions.

However, the influence of MBP and P2 on membrane dynamics investigated in this study is not significant. In relation to this, we should mention that for our previous study on P2 effects in a liposome system, much higher protein concentrations were used (1.25% (w/w); protein : lipid ratio 1 : 1500). Furthermore, neutron diffraction data showed that the structure of large membrane fractions is affected by the two myelin proteins, even at low concentration.

Conclusions

The influence of the myelin proteins MBP and P2 on structure and dynamics of reconstituted model myelin membranes was investigated by neutron diffraction and quasi-elastic neutron scattering. The diffraction measurements revealed that, in the lipid gel phase, protein-containing membranes exhibit the same *d*-spacing as the lipids, suggesting that they have minimal effect on the structure. In contrast, in the liquid phase, the proteins were shown to significantly increase the interbilayer distances. A model was suggested, in which MBP widens the interbilayer space and penetrates ~2 Å into opposing bilayers. P2-containing membranes were found to exhibit two widened membrane fractions. The larger spacing is suggested to contain P2, penetrating partially into the bilayer. In combination, MBP and P2 result in the same *d*-spacings as P2 alone. Due to a threefold excess of P2 with respect to MBP, it is possible that proteins assemble within the membrane in synergy. When MBP and P2 were included in the membrane separately, each protein was shown to induce an additional, less ordered, membrane fraction with a large *d*-spacing, particularly in the gel phase, consistent with proteins being squeezed out.[51] This was absent when added together, suggesting that the proteins can act together to increase bilayer stacking.[29]

Five different hydrogen populations were necessary to model the quasi-elastic spectra in the liquid phase: (1) a fraction that undergoes only vibrational motions and appears immobile

within the experimental resolution, (2 and 3) two populations that diffuse in a confined spherical volume and belong to the initial and terminal parts of the lipids, respectively, (4) a hydrogen fraction belonging to methylene groups that undergoes 2-site jump diffusion and (5) fraction described by an additional Lorentzian. MBP was found to enhance the diffusive motions of the lipids, according to the structural properties of this membrane sample: due to the widening of the interbilayer spacing induced by MBP, which penetrates into the bilayer, the lipids were suggested to be more flexible, resulting in increased diffusive motions. Unlike MBP, P2 did not appear to significantly affect the diffusive motions of the lipids. This was explained by the compensating structural and electrostatic properties of P2: although an increase in interbilayer spacing was observed, which could increase flexibility, the positive electrostatic potential of P2, concentrated at the two opposing sides of the protein, is suggested to compensate the enhancement of the dynamics, because of strong stabilizing electrostatic protein–lipid interactions. MBP and P2 present together in a membrane have shown to affect the lipid-motions in the terminal part of the lipids, while the initial part remained unaffected: the diffusion constant of the hydrogen population belonging to the terminal part of the lipids was found to be reduced for the out-of-plane configuration. This effect is consistent with the previously proposed synergistic stacking effect of multilayers induced by MBP and P2 by Suresh *et al.*[29] In contrast, the diffusion constant of the hydrogen population belonging to the initial part of the lipids remained unaffected by the proteins, which could be explained by the proposed association of MBP and P2 based on the neutron diffraction data, where the MBP proteins would have to penetrate deeply into the bilayer. This could widen the interbilayer spacing and thus increase the membrane dynamics. In contrast, the strong electrostatic interactions between MBP–P2 protein assemblies and the lipids caused by the positive charge distribution of P2 proteins, concentrated on the opposing sides of the protein, would decrease the flexibility, and thus increased membrane dynamics remain compensated.

In summary, these results propose a model in which the myelin-specific proteins MBP and P2 associate within the interbilayer space of a reconstituted myelin membrane and influence the structure of large membrane fractions, whereas membrane dynamics do not change significantly at the low protein concentrations used in the current study. MBP and P2 are suggested to promote adhesion between the bilayers, caused by electrostatic interactions and a synergistic stacking effect by both proteins. This could play an important role in the formation and stability of compacted PNS myelin and its major dense line. For the future, further myelin proteins and lipids will be added gradually, in order to investigate more complex model myelin membranes that are closer to natural myelin.

Acknowledgements

We are grateful for ILL for beamtime and financial support. Further thanks go to the European Commission, which supported the performance of experiments carried out at HZB and to the Science and Technology Facilities Council (STFC), UK, for access to the ISIS Facility and beamtime. We would like to express our gratitude to DESY, the IBS and the EMBL for using their laboratories for the sample preparation and in particular to Iulia Blesniac and Juliette Devos for their help during sample characterization. Moreover, the responsible scientists for the DSC and the DLS instruments, Isabelle Grillo and Ralf Schweins, also deserve our thanks, especially for using the chemical laboratory.

Notes and references

1 G. W. Brady, N. S. Murthy, D. B. Fein, D. D. Wood and M. A. Moscarello, *Biophys. J.*, 1981, **34**, 345–350.
2 R. H. Quarles, W. B. Macklin and P. Morell, in *Basic Neurochemistry: Molecular, Cellular and Medical Aspects*, Academic Press Elsevier, New York, 2006, ch. 4, pp. 51–71.
3 C. M. Taylor, C. B. Marta, R. Bansal and S. E. Pfeiffer, in *Myelin Biology and Disorders*, Elsevier Academic Press, San Diego, CA, 2004.
4 S. Greenfield, S. Brostoff, E. H. Eylar and P. Morell, *J. Neurochem.*, 1973, **20**(4), 1207–1216.
5 O. Jahn, S. Tenzer and H. B. Werner, *Mol. Neurobiol.*, 2009, **40**, 55–72.
6 J. Patzig, O. Jahn, S. Tenzer, S. P. Wichert, P. de Monasterio-Schrader, S. Rosfa, J. Kuharev, K. Yan, I. Bormuth, J. Bremer, A. Aguzzi, F. Orfaniotou, D. Hesse, M. H. Schwab, W. Möbius, K.-A. Nave and H. B. Werner, *J. Neurosci.*, 2011, **31**(45), 16369–16386.
7 J. A. Benjamins and P. Morell, *Neurochem. Res.*, 1978, **3**, 137–174.
8 N. Baumann and D. Pham-Dinh, *Physiol. Rev.*, 2001, **81**(2), 871–927.
9 P. Riccio, L. Masotti, P. Cavatorta, A. De Santis, D. Juretic, A. Bobba, J. Pasquali-Ronchetti and E. Quagliariello, *Biochem. Biophys. Res. Commun.*, 1986, **134**(1), 313–319.
10 C. Readhead, B. Popkoa, N. Takahashia, H. D. Shinea, R. A. Saavedraa, R. L. Sidmana and L. Hooda, *Cell*, 1987, **48**, 703–712.
11 G. Harauz, V. Ladizhansky and J. M. Boggs, *Biochemistry*, 2009, **48**, 8094–8104.
12 G. Harauz, N. Ishiyama, C. M. D. Hill, I. R. Bates, D. S. Libich and C. Farès, *Micron*, 2004, **35**, 503–542.
13 V. Majava, C. Wang, M. Myllykoski, S. M. Kangas, S. U. Kang, N. Hayashi, P. Baumgärtel, A. M. Heape, G. Lubec and P. Kursula, *Amino Acids*, 2010, **39**, 59–71.
14 C. Wang, U. Neugebauer, J. Brück, M. Myllykoski, P. Baumgärtel, J. Popp and P. Kursula, *PLoS One*, 2011, **6**(5), e19915.
15 W. R. Krigbaum and T. S. Hsu, *Biochemistry*, 1975, **14**, 2542–2546.
16 E. Polverini, A. Fasano, F. Zito, P. Riccio and P. Cavatorta, *Eur. Biophys. J.*, 1999, **28**, 351–355.
17 H. Haas, M. Torrielli, R. Steitz, P. Cavatorta, R. Sorbi, A. Fasano, P. Riccio and A. Gliozzi, *Thin Solid Films*, 1998, **327–329**, 627–631.

18 D. R. Beniac, M. D. Luckevich, G. J. Czarnota, T. A. Tompkins, R. A. Ridsdale, F. P. Ottensmeyer, M. A. Moscarello and G. Harauz, *J. Biol. Chem.*, 1997, **272**(7), 4261–4268.
19 R. A. Ridsdale, D. R. Beniac, T. A. Tompkins, M. A. Moscarello and G. Harauz, *J. Biol. Chem.*, 1997, **272**(7), 4269–4275.
20 V. Majava, E. Polverini, A. Mazzini, R. Nanekar, W. Knoll, J. Peters, F. Natali, P. Baumgärtel, I. Kursula and P. Kursula, *PLoS One*, 2010, **5**, e10300.
21 I. R. Bates, J. B. Feix, J. M. Boggs and G. Harauz, *J. Biol. Chem.*, 2004, **279**, 5757–5764.
22 E. Polverini, E. P. Coll, D. P. Tieleman and G. Harauz, *Biochim. Biophys. Acta, Biomembr.*, 2011, **1808**(3), 674–683.
23 J. M. Boggs, M. A. Moscarello and D. Papahadjopoulos, in *Lipid-protein interactions*, Wiley-Interscience, New York, 1982.
24 M. B. Sankaram, P. J. Brophy and D. Marsh, *Biochemistry*, 1989, **28**, 9699–9707.
25 P. Morell, R. H. Quarles and W. T. Norton, in *Basic Neurochem.*, ed. Raven, New York, 1997, pp. 117–143.
26 B. D. Trapp, M. Dubois-Dalcq and R. H. Quarles, *J. Neurochem.*, 1984, **43**(4), 944–948.
27 P. Dupouey, C. Jacque, J. M. Bourre, F. Cesselin, A. Privat and N. Baumann, *Neurosci. Lett.*, 1979, **12**, 113–118.
28 J. Rosenbluth, *J. Comp. Neurol.*, 1980, **193**, 729–739.
29 S. Suresh, C. Wang, R. Nanekar, P. Kursula and J. M. Edwardson, *Biochemistry*, 2010, **49**, 3456–3463.
30 H. Han, M. M. Myllykoski, S. Ruskamo, C. Wang and P. Kursula, *BioFactors*, 2013, **39**, 233–241.
31 P. Riccio, F. Zito, A. Fasano, G. M. Liuzzi, F. Lolli, E. Polverini and P. Cavatorta, *NeuroReport*, 1998, **9**, 2769–2773.
32 W. Knoll, F. Natali, J. Peters, R. Nanekar, C. Wang and P. Kursula, *Spectroscopy*, 2010, **24**(6), 585–592.
33 I. R. Bates, P. Matharu, N. Ishiyama, D. Rochon, D. D. Wood, E. Polverini, M. A. Moscarello, N. J. Viner and G. Harauz, *Protein Expression Purif.*, 2000, **20**, 285–299.
34 F. W. Studier, *Protein Expression Purif.*, 2005, **41**(1), 207–234.
35 M. Hammarström, E. A. Woestenenk, N. Hellgren, T. Härd and H. Berglund, *J. Struct. Funct. Genomics*, 2006, **7**, 1–14.
36 http://www.ill.eu/instruments-support/instruments-groups/instruments/d16/description/instrument-layout/.
37 http://www.ill.eu/instruments-support/instruments-groups/instruments/in16/.
38 http://www.ill.eu/instruments-support/computing-for-science/cs-software/all-software/lamp.
39 http://www.isis.stfc.ac.uk/instruments/iris/data-analysis.
40 J. Fitter, B. Rufflé and R. E. Lechner, *FITMO: NEAT software package*.
41 M. Bée. *Quasi-elastic Neutron Scattering*, Adam Hilger, 1988.
42 F. Volino and A. J. Dianoux, *Mol. Phys.*, 1980, **41**(2), 271–279.
43 T. Springer, *Springer Tracts in Modern Physics*, Springer, 1972, vol. 64.
44 Y. Gerelli, V. G. Sakai, J. Ollivier and A. Deriu, *Soft Matter*, 2011, **7**(8), 3929–3935.
45 F. James and M. Winkler, *Minuit Users Guide*, CERN, Geneva, 2004.
46 C. D. Hodgman. *Handbook of Chemistry and Physics*. Chemical Rubber Publishing Company, 1952.
47 T. C. Hansen, M. M. Koza and W. F. Kuhs, *J. Phys.: Condens. Matter*, 2008, **20**, 285104.
48 T. C. Hansen, M. M. Koza, P. Lindner and W. F. Kuhs, *J. Phys.: Condens. Matter*, 2008, **20**, 285105.
49 L. Bosio, G. P. Johari and J. Teixeira, *Phys. Rev. Lett.*, 1986, **56**(5), 460–463.
50 R. G. Oliveira and B. Maggio, *Biochim. Biophys. Acta*, 2002, **1561**, 238–250.
51 C. M. Rosetti, B. Maggio and R. G. Oliveira, *Biochim. Biophys. Acta*, 2008, **1778**, 1665–1675.
52 J. F. Nagle and S. Tristram-Nagle, *Biochim. Biophys. Acta*, 2000, **1469**, 159–195.
53 H. I. Petrache, S. Tristram-Nagle, K. Gawrisch, D. Harries, V. A. Parsegian and J. F. Nagle, *Biophys. J.*, 2004, **86**, 1574–1586.
54 W. Pfeiffer, T. Henkel, E. Sackmann, W. Knoll and D. Richter, *Europhys. Lett.*, 1989, **8**(2), 201–206.
55 M. Trapp, T. Gutberlet, F. Juranyi, T. Unruh, B. Demé, M. Tehei and J. Peters, *J. Chem. Phys.*, 2010, **133**, 164505.
56 J. Swenson, F. Kargl, P. Berntsen and C. Svanberg, *J. Chem. Phys.*, 2008, **129**, 045101.
57 J. Fitter, R. E. Lechner, G. Buldt and N. A. Dencher, *Proc. Natl. Acad. Sci. U. S. A.*, 1996, **93**(15), 7600–7605.
58 M. Doxastakis, V. G. Sakai, S. Ohtake, J. K. Maranas and J. J. De Pablo, *Biophys. J.*, 2007, **92**(1), 147–161.
59 M. F. Brown, J. Seelig and U. Häberlen, *J. Chem. Phys.*, 1979, **70**, 5045–5053.
60 M. C. Pitman, F. Suits, K. Gawrisch and S. E. Feller, *J. Chem. Phys.*, 2005, **122**, 244715.
61 D. P. Tieleman, S. J. Marrink and H. J. C. Berendsen, *Biochim. Biophys. Acta Biomembr.*, 1997, **1331**(3), 235–270.
62 D. Djurado, M. Bée, M. Sniechowski, S. Howells, P. Rannou, A. Pron, J. P. Travers and W. Luzny, *Phys. Chem. Chem. Phys.*, 2005, **7**, 1235–1240.
63 F. Natali, A. Gliozzi, R. Rolandi, A. Relini, P. Cavatorta, A. Deriu, A. Fasano and P. Riccio, *Appl. Phys. A*, 2002, **74**, S1582–S1584.
64 F. Natali, A. Relini, A. Gliozzi, R. Rolandi, P. Cavatorta, A. Deriu, A. Fasano and P. Riccio, *Chem. Phys.*, 2003, **292**, 455–464.
65 F. Natali, A. Relini, A. Gliozzi, R. Rolandi, P. Cavatorta, A. Deriu, A. Fasano and P. Riccio, *Phys. B*, 2004, **350**, e623–e626.
66 M. J. Janiak, D. M. Small and G. G. Shipley, *J. Biol. Chem.*, 1979, **254**(13), 6068–6078.
67 M. Weik, U. Lehnert and G. Zaccai, *Biophys. J.*, 2005, **89**(5), 3639–3646.